

SIZE DEPENDENT REFLECTIVE PROPERTIES OF TiO₂ NANOPARTICLES AND REFLECTORS MADE THEREOF

SANJEEV KUMAR^{a*}, N. K. VERMA^a, M. L. SINGLA^b

^a*School of Physics and Materials Science, Thapar University, Patiala, India*

^b*Central Scientific Instruments Organisation, Chandigarh, India*

The present work investigates the size dependent reflective properties of TiO₂ nanoparticles and discusses the development of reflectors. The nanocrystalline TiO₂ powders with different crystallinity and phase structures were obtained by controlling the reaction parameters. TiO₂ nanoparticles synthesized via sol-gel method were characterized by using X-ray diffraction (XRD), transmission electron microscope (TEM), UV-Vis absorption fluorospectrophotometer and UV-Vis diffuse reflectance spectroscopy (UV-Vis DRS). Rutile phase TiO₂ nanoparticles with crystallite sizes in the range, 77.50 - 78.31 nm, were obtained by adjusting the L value in the range 20 to 50. On calcining the TiO₂ powders from 350°C to 900°C, the particle size increases from 60 to 150 nm and band gap energy decreases from 3.42 to 3.14 eV, calculated respectively using TEM micrograph and UV-Vis absorption spectra. PL spectrum shows a broad luminescence peak at 431 nm, irrespective of the different calcination temperatures. TiO₂ nanoparticles with L value of 40 shows the attainment of maximum diffuse reflectance (99.50 - 99.60%). Employing these nanoparticles as reflective pigment, coating material was prepared and applied on plastic substrate with different coating thicknesses to develop reflectors. These reflectors show maximum diffuse reflectance, 97.12 - 96.91%, for the 0.25-mm thick coating with 17% pigment to binder weight ratio.

(Received January 12, 2012; Accepted April 24, 2012)

Keywords: Reflective coatings, TiO₂ nanoparticles, Rutile phase, diffuse reflectance

1. Introduction

Reflective coatings are used in a wide variety of applications such as automobiles, buildings, luminaries [1, 2]. The coating protects the substrate from degradation as well as serves as a light reflector. Reflective coating formulation usually contains a number of components [2]. A primary component is a reflective pigment, which imparts a pleasing color and reflective properties to various media in which it is mixed, such as paints, organic resins, varnishes. Secondary component is a binder, which can be natural or synthetic, used to bind the pigment to a substrate and provides durability to the coatings. Titanium dioxide (TiO₂) is mainly used as white reflective pigment in these types of coatings [3].

The naturally occurring oxide of Titanium at atmospheric pressure exhibits three polymorphs: anatase, brookite and rutile. The anatase phase is used for photocatalysis due to its high photoreactivity [4]. Brookite phase is difficult to produce and therefore has no importance in the pigment industry [5]. Rutile phase is thermodynamically the most stable and possesses the highest density with compact atomic structure [6]. TiO₂ having rutile phase is largely employed as reflective pigment in the reflective coatings [7, 8] because of its effective light scattering properties. Coatings containing even small amount of TiO₂ (rutile phase) particles reflect almost the entire visible light.

* Corresponding author: kumarsanju25@gmail.com

Mechanism of reflectance by an isolated particle can be studied by Mie theory [9]. It depends upon the refractive index, band gap, shape, size, and surface characteristics of the particles [9, 10]. In reflective coatings, the properties of particles are significantly altered on mixing with other materials (binder, solvent, etc.) [9]. The reflectance of coatings depends upon the relative refractive index of the particles and that of their surrounding medium, distribution of particles in the coating, loading of particles, binder concentration and wavelength of the incident light [11].

As of today, the reflective coatings used are of conventional type, which employ bulk TiO₂ particles of about 0.1 μm size as reflective pigment. These pigments are prepared by crushing the minerals obtained from their respective ores; after crushing, aggregated crystals are shattered into small granules. This results in individual particles of irregular shape and size. Not only do the particles vary in shape and size, but also in their composition. The mineral contains inclusions, which are less in amount and act as impurities [12]. As a result, materials absorb certain wavelengths of visible light and their reflective property deteriorates. To date, these materials are used as reflective pigments and they barely meet the aforementioned requirements for the reflective coatings. Moreover, the bulk TiO₂ particles show diffuse reflectance in the range of 90-91% [13].

Coating material containing nanoparticles significantly enhances the properties of the various coatings, such as: scratch-resistant, UV protective, antibacterial [14, 16]. Applications of nanoparticles are expanding at a rapid rate because of their unique and excellent properties [17, 18]. Due to controlled morphology [19, 20], high surface to volume ratio and high purity, TiO₂ nanoparticles are apparently potential candidates for reflective coatings as compared to its bulk counterpart.

From the extensive survey of past studies on the TiO₂ nanoparticles, it has been observed that the synthesis of uniform crystalline nanoparticles with different size and shape have been reported by many researchers [21-23]. But the effect of controlling the morphology of these nanoparticles on the reflective properties has not been explored. And, to the best of our knowledge, no one has reported the work on the reflective coatings, based on the TiO₂ nanoparticles. The present work aims at the study of size dependent reflective properties of TiO₂ nanoparticles and the reflector made thereof.

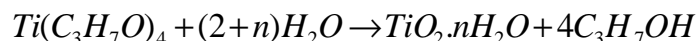
2. Experimental

2.1 Synthesis of TiO₂ nanoparticles

Analytical grade of Titanium isopropoxide Ti(OCH(CH₃)₂)₄, anhydrous 2-propanol (C₃H₈O) were procured from SIGMA-Aldrich, whereas acrylic binder (VISYCRYL-8350) from N. R. Chemicals.

Sol-gel technique has been used to synthesize TiO₂ nanoparticles at room temperature [4]. In a typical experiment, titania isopropoxide was dissolved in 100 ml of anhydrous 2-propanol (0.4 M). A measured quantity of distilled water was mixed with 100 ml of anhydrous 2-propanol to prepare a second solution. Both the solutions were covered and stirred for 45 minutes. With the help of a burette, the water solution was added drop-wise to the first solution under constant magnetic stirring for another 6 hours. As a result of hydrolysis of titania isopropoxide, the color of solution changed from transparent to white indicating the formation of precipitates. Different solutions were prepared by varying the L (ratio of molar concentration of water to that of alkoxide precursor) within the range of 20 - 50.

The reaction of hydrolysis of the titania isopropoxide proceeds as follows:



The precipitates were filtered and dried in an oven at 60°C for 8 hours; after crushing in pestle and mortar, powder of titania was obtained. The dried powder was then calcined at 350°C,

550°C, 750°C and 900°C for 15 minutes to remove the solvent completely as well as to crystallize the amorphous titania powder.

2.2. Preparation of coating materials

Coating materials were prepared by dispersing TiO₂ nanoparticles in de-ionized water solution of organic binder with different pigment to binder weight ratios (Table 1). Particularly, 2.0 g of TiO₂, 0.24 g of product VISYCRYL- 8350, and 4.0 gm of de-ionized water were mixed using Planetary Ball Mill, for 5 minutes at 800-1000 rpm. The pH of the coating material was adjusted in-between 6 to 8.

Table 1: Preparation of different coating materials with different pigment to binder weight ratio.

Coating material	Pigment to binder weight ratio (%)	Pigment to solvent weight ratio
TiO ₂ :A	8.3:1 (12%)	1:2
TiO ₂ :B	7.1:1 (14%)	1:2
TiO ₂ :C	6.1: 1 (16%)	1:2

2.3 Development of reflectors

Plastic sheet (2cm x 2cm), having thickness of 1 mm was used as substrate, mechanically sanded, cleaned using detergent, rinsed with de-ionized water and isopropyl alcohol. These sheets were spray coated with the coating material with different thicknesses. Before applying the coating material, a thin layer of binder was applied to the substrate for better adhesion. The coating was done by spreading one layer over the other to develop reflectors; care was taken to apply the second layer before the glossy appearance of the first layer disappeared.

2.4 Characterization of TiO₂ nanoparticles

PANanalyticals X'Pert Pro X-ray diffractometer was employed to determine the phase purity and crystal structure of the synthesised nanoparticles. Size and morphology of the nanoparticles were studied through Hitachi (H-7500) transmission electron microscope (TEM). Perkin Elmer (350) UV-Visible spectrophotometer was used to record optical absorption spectra and, Cary Varian fluorospectrophotometer, to measure photoluminescence (PL).

2.5 Measurement of diffuse reflectance

The diffuse reflectance measurement of the nanoparticles was performed by UV-Visible spectrophotometer, attached with integrating sphere to spatially integrate the radiant flux. For the measurement, the nanoparticles were pressed into thick pellet, and placed at the entrance port of the integrating sphere. The same set up was used to measure diffuse reflectance of the developed reflectors. Calibration of the reflectance scale was done by standard reference material (WS-1-SL, Spectralon).

3. Results and discussion:

The XRD patterns of TiO₂ powder calcined at different temperatures are shown in Fig. 1. The peaks indexed to the reflection from (110), (101), (200), (111), (210), (211), (220), (002), and

(310) planes, at 2θ values 27.54° , 36.04° , 39.20° , 41.12° , 44.14° , 54.33° , 56.89° , 62.82° , and 64.17° correspond to rutile phase of TiO_2 (JCPDS card #860148) as well as, the reflection from (101), (004), (200), (105), (211) and (204) planes, at 2θ values 25.44° , 38.02° , 48.19° , 53.94° , 54.98° , and 63.06° correspond to anatase phase of TiO_2 (JCPDS card #861157). Fig. 1(a) is the

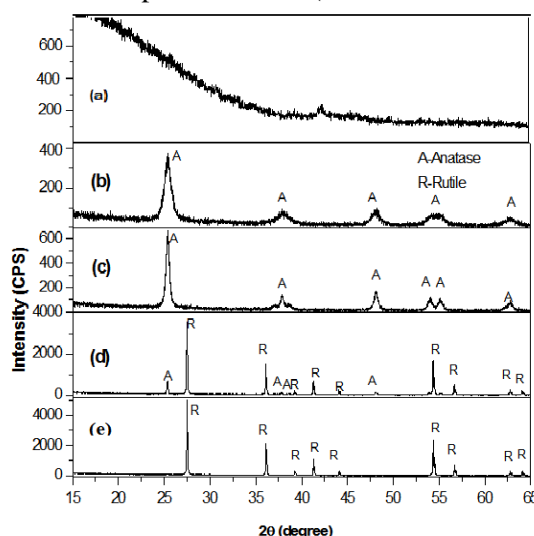


Fig. 1: X-ray diffraction patterns of TiO_2 powder (a) uncalcined and calcined at (a) 350°C (b) 550°C (c) 750°C (d) 900°C .

X-ray diffraction (XRD) pattern of the uncalcined titania powder, indicating its amorphous nature. The amorphous phase could be hydrous TiO_2 , i.e., $\text{TiO}_2 \cdot n\text{H}_2\text{O}$. Figs. 1(b) and (c) reveal that samples calcined at 350°C and 550°C exhibit characteristic peaks of only anatase phase, while the sample calcined at 750°C (Fig.1(d)) exhibit peaks of both anatase and rutile phase. Examination of the kinetics of the anatase to rutile phase transformation involves the assessment of the relative quantities of anatase and rutile weight fraction at 750°C . The weight fraction (W_R) of rutile phase content calcined at 750°C (Fig. 1(d)) was calculated from the equation (1) [24]

$$W_R = \frac{1}{(1 + I_A / 0.886I_R)} \quad (1)$$

where I_A and I_R are the intensity of most intense peaks of anatase and rutile phase respectively. Substituting the values of I_A and I_R from Fig. 1(d), W_R for rutile phase is 83%. Mixed-phases (rutile–anatase) of TiO_2 have been reported to exhibit enhanced photoactivity relative to single-phase titania [25]. It is considered widely that this is the result of improved charge carrier separation, possibly through the trapping of electrons in rutile and the consequent reduction in electron–hole recombination [26].

With the further increase in the calcination temperature, i.e., 750°C to 900°C the formation of complete rutile phase has been observed. From the XRD patterns (Fig. 1(d, e)), it is clear that with increase in calcination temperature, the peak broadening decreases and phase transformation from anatase to rutile registers incline. The anatase to rutile transformation is reconstructive, which means that the transformation involves the breaking and reforming of bonds [27]. This is in contrast to the displacive transformation, in which the original bonds are distorted but retained. The reconstructive anatase to rutile transformation involves a contraction of the c-axis and an overall volume contraction of 8% [28]. This volume contraction explains the higher density of rutile relative to anatase. For the transformation of anatase to rutile phase a sufficient amount of thermal energy is required to facilitate the rearrangement of atoms. It has been reported that for typical bulk TiO_2 powders this energy requirement is obtained at $600\text{--}700^\circ\text{C}$ in air in the absence of any dopants or impurities. However, the reported transition temperature varies in the range $400\text{--}1200^\circ\text{C}$, owing to the use of different methods of determining the transition

temperatures, raw materials and processing techniques. The anatase to rutile transformation is not instantaneous; it is time-dependent because it is reconstructive. This transformation temperature can be enhanced or impeded by influencing the rearrangement of the atoms in the anatase and rutile lattices. It has been reported that the most important factor affecting the phase transformation is the presence and amount of oxygen defects in the titania lattice [29]. Ease of rearrangement and transformation are enhanced by relaxation of the large oxygen sublattice through the increased presence of oxygen vacancies [30].

Table 2: Nanoparticle-crystallite size variation with calcination temperatures.

Sr. No.	Sample & Calcination temperature (°C)	Crystallite size (nm)
(a)	TiO ₂ : 350	29.31
(b)	TiO ₂ : 550	49.16
(c)	TiO ₂ : 750	73.25
(d)	TiO ₂ : 900	77.50

Table 2 shows the crystallite sizes of the samples calcined at different temperatures, calculated using Debye Scherrer's equation [23]. Crystallite size is determined by measuring the broadening of a particular peak in the diffraction pattern associated with a particular planar reflection from within the crystal unit cell. It is inversely related to the full width at half maximum (FWHM) of an individual peak; narrower the peak, larger the crystallite size. The periodicity of the individual crystallite domain reinforces the diffraction of the X-ray beam, resulting in a tall narrow peak. If the crystals are randomly arranged or have low degrees of periodicity, the result is a broader peak [23]. This is normally the case for nanomaterial assemblies. Thus, it is apparent that the FWHM of the diffraction peak is related to the size of the nanomaterials. The FWHM has been calculated from the most intense peak (Fig. 1), using Lorentz best fit curve ($R^2 > 0.98$). It is clear from Table 2 that with increase in the calcination temperature, the crystallite size increases.

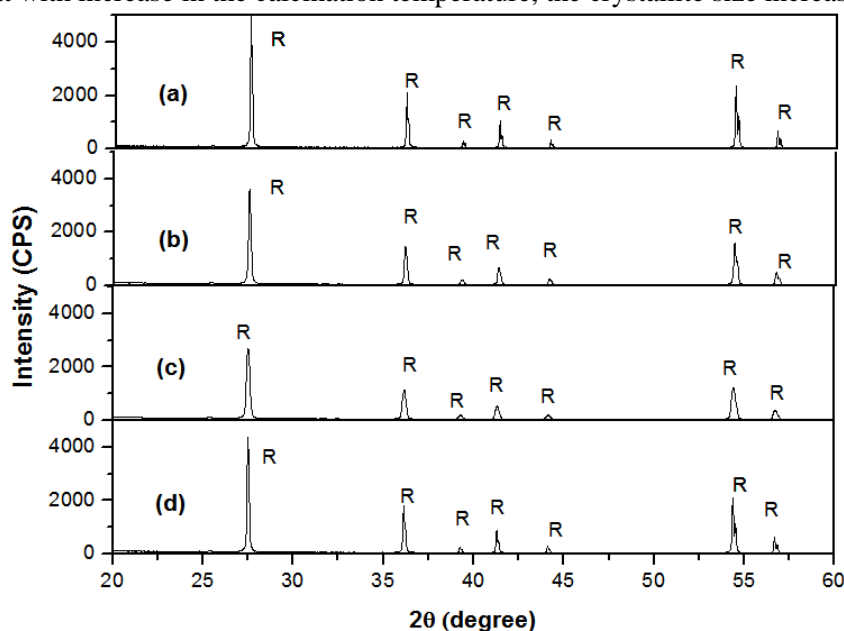


Fig. 2: X-ray diffraction patterns of TiO₂ nanoparticles calcined at 900°C with different L values (a) 20 (b) 30 (c) 40 (d) 50.

Fig. 2 shows the X-ray diffraction pattern of TiO₂ nanoparticles calcined at 900°C with different L values. All the peaks are well matched with rutile phase of TiO₂ (JCPDS card #860148). As observed from the XRD pattern, with increase in the L value i.e., from 20 to 40,

there is an increase in the peak broadening but with further increase in the L value from 40 to 50, depreciation takes place. Table 3 shows the crystallite sizes of the samples calcined at 900°C, with different L values calculated using Debye Scherrer's equation.

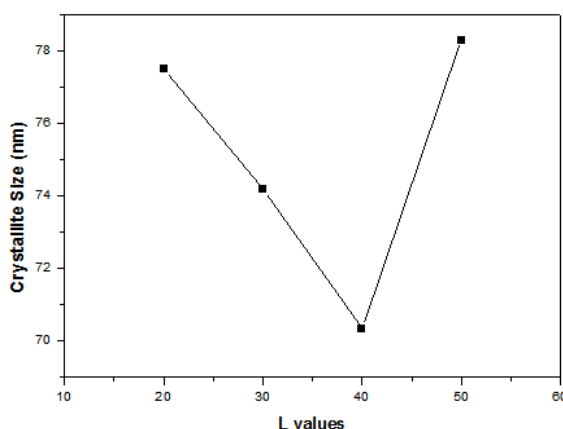


Fig. 3: Nanoparticles crystallite size variation with L values.

Fig. 3 shows the graphical variation of crystallite size with L values for TiO₂ nanoparticles calcined at 900°C. As observed from the Fig. 3, with increase in the L values from 20 to 40, there is decrease in the crystallite size and with further increase in the L values from 40 to 50, the crystallite size increases.

Table 3: Nanoparticle-crystallite size variation with L values.

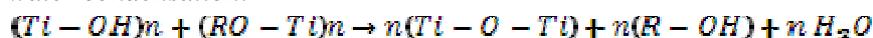
Sr. No.	L values	Crystallite size (nm)
(a)	20	77.50
(b)	30	74.20
(c)	40	70.34
(d)	50	78.31

For the formation of TiO₂ nanoparticles, the net reaction is shown below.

Hydrolysis:



Alcohol and water condensation:



As clear from the above reactions, the nucleation rate of TiO₂ particles increases with increasing L, and as a result, the average nanocrystallite size and the average nanoparticle size should decrease with increasing L (Table 3). In addition to this, with increasing L, although the hydrolysis reaction in the above equation is driven in the forward direction, the condensation reaction driven in the reverse direction, which suggests more dissolution of TiO₂ particles, which effectively reduce the average size of nucleated TiO₂ particles. However, due to the formation of large number of nuclei with increasing L, the growth rate of the TiO₂ nanocrystallites also increases [4].

The size and morphology of TiO₂ nanoparticles was investigated by TEM. The values of H₂O/titanium (L) precursor and calcination temperatures are significant parameters in controlling TiO₂ particle size and size distribution. In the present study, both the parameters were utilized to control the morphology of TiO₂ nanoparticles. Fig. 4 shows the TEM micrographs of uncalcined TiO₂. It reveals that the uncalcined particles get aggregated and coalesce non-uniformly because of cohesive force of TiO₂ nanoparticles.

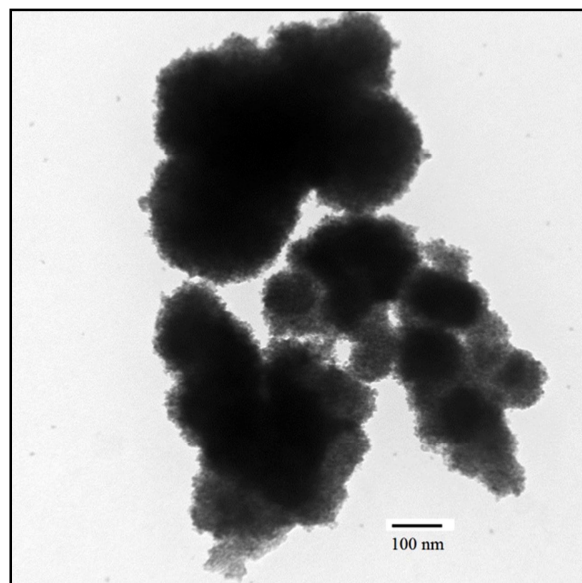


Fig. 4: TEM micrograph of uncalcined TiO_2 nanoparticles.

Amorphous TiO_2 nanoparticles have been transformed into anatase when heated at temperature from 350°C to 550°C (XRD study). Fig. 5 shows the TEM micrographs of TiO_2 nanoparticles calcined at different temperatures. According to the micrographs, the particles are found to be uniformly distributed and nearly spherical. This might be due to the decrease in the cohesive force of TiO_2 nanoparticles with the increase of the average diameter of TiO_2 nanoparticles [31]. With the increase in the calcination temperature from 350°C to 550°C , the particle size increases (Table 4)

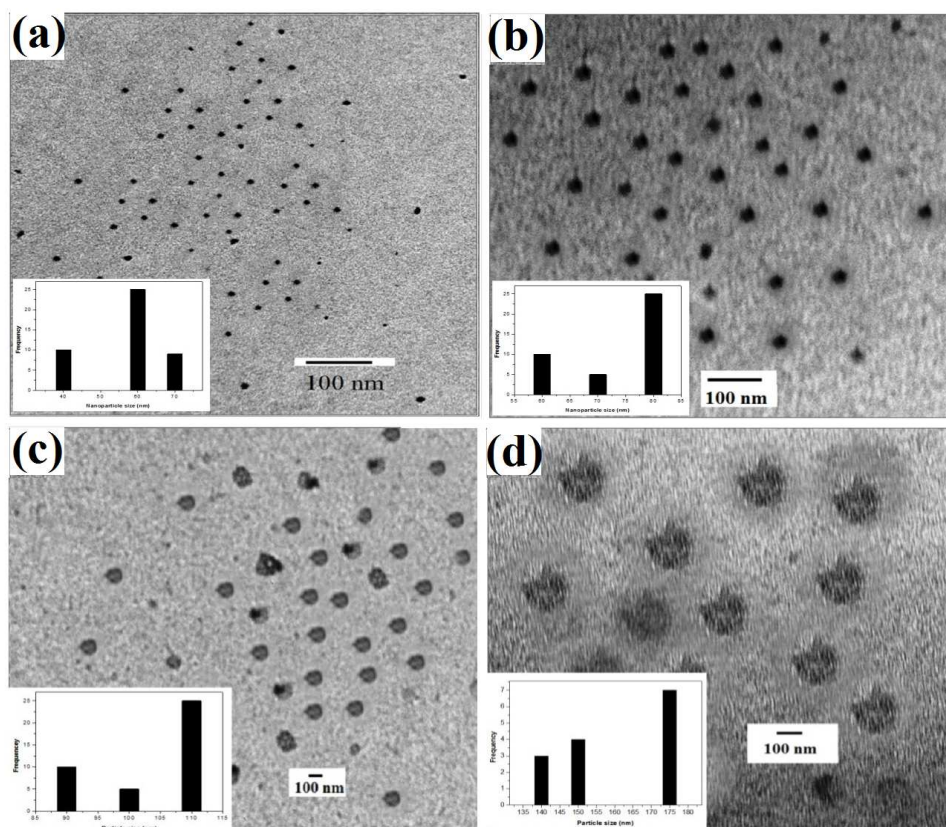


Fig. 5: TEM micrographs of TiO_2 nanoparticles calcined at (a) 350°C (b) 550°C (c) 750°C (d) 900°C .

With further increase in the calcination temperature from 750°C to 900°C, the particle size increases (Table 4). The average size (Table 4) of calcined particles has been calculated from TEM micrographs by plotting histograms. Significant rutile grain growth is exhibited as the anatase to rutile transition proceeds. Rutile grains coarsen at the expense of neighboring anatase during coalescence until the large rutile grains begin to impinge on each other [32]. This increase in grain size causes a decrease in surface area leading to decrease in photocatalytic activity and increase in the photostability of TiO₂ nanoparticles. It can be observed (Table 4) that the heat treatment of the nanopowders largely affects the domain size, as calculated through TEM micrographs, it increased from 60 nm for the as-synthesized nanopowders up to 175 nm for the TiO₂ treated at 900°C.

Table 4: Particle size variation with calcination temperature.

Sr. No.	Sample & Calcination temperature (°C)	Particle size (nm)
(a)	TiO ₂ : 350	60
(b)	TiO ₂ : 550	80
(c)	TiO ₂ : 750	110
(d)	TiO ₂ : 900	175

Fig. 6 shows the uv-visible absorption spectra of the TiO₂ nanoparticles calcined at different temperatures. The spectra reveal that with increase in calcination temperature; the absorption edge gets shifted to higher wavelength (red shift).

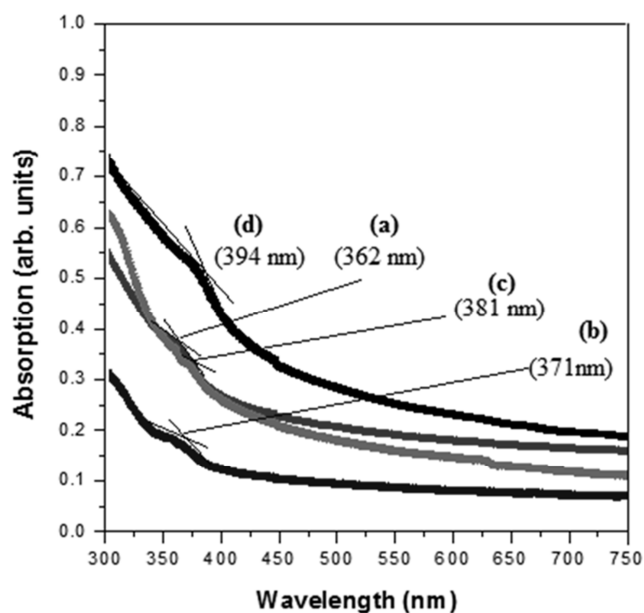


Fig. 6: UV-Vis absorption spectra of TiO₂ nanoparticles calcined at (a) 350°C (b) 550°C (c) 750°C (d) 900°C

The band gap energies (E_g) of TiO₂ nanoparticles were calculated using the equation (2) [33, 34]

$$E_g = \frac{hc}{\lambda_{int}} \quad (2)$$

where h is Planck's constant (4.135×10^{-6} eV.nm); c , the velocity of light (3×10^8 m s⁻¹), and λ_{int} , the wavelength (in nm) corresponding to the intersection of extension of linear parts of the spectrum of y-axis and x-axis. From Fig. 6, the energy band gap values for TiO₂ nanoparticles

calcined at different temperature were found to be in the range of 3.14 - 3.42 eV (Table 5). The crystallite size of rutile phase nanocrystalline TiO₂ increases with respect to calcination temperature (XRD study), leading to decrease in the energy band-gap values (Table 5). Small band-gap values are indicative of relatively densely packed crystalline structures. It is well known that the band-gap of a semiconductor decreases with increase in the crystallite size of TiO₂ [7]. Generally, the color of a solid is determined by the position of its absorption edge; a shift of this absorption edge towards a higher wavelength can result in absorption in the visible region.

Table 5 Determination of band gap energy of TiO₂ nanoparticles calcined at different temperatures.

Sr. No.	Sample & Calcination temperature (°C)	Band gap energy (eV)
(a)	TiO ₂ : 350	3.42
(b)	TiO ₂ : 550	3.34
(c)	TiO ₂ : 750	3.25
(d)	TiO ₂ : 900	3.14

PL emission spectra have been widely used to investigate the efficiency of charge carrier trapping and migration, and to understand the fate of electron-hole pairs in semiconductors [35] Fig. 7 shows the PL spectra of TiO₂ nanoparticles calcined at different temperatures, at an excitation wavelength of 370 nm. As seen from the spectra, a broad peak at 431 nm is observed for all the samples, irrespective of the different calcination temperature. This emission band originated from charge recombination at the shallow-trap surface state [36]. These surface states originate from the oxygen vacancies which act as radiative centers.

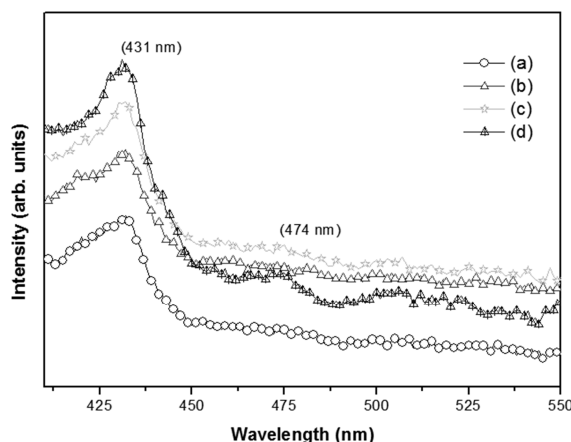


Fig. 7: Room temperature photoluminescence emission spectra of TiO₂ nanoparticles calcined at (a) 350°C (b) 550°C (c) 750°C (d) 900°C, at an excitation wavelength of 370 nm.

The peak around 474 nm for TiO₂ nanoparticles is due to the oxygen vacancy with two trapped electrons, i.e., F centers [37]. These defect states play an important role in determining the reflective properties and photocatalytic properties of TiO₂ nanoparticles. In the manufacturing process of titanium dioxide pigment, it is aimed to obtain a product with the highest photostability and lowest photocatalytic activity [38, 39]. This can be realized in various ways, and the techniques can be divided into two fundamental groups. The first group comprises of the methods that prevent the migration of electrons and holes to the surface of TiO₂, and the second group comprises of the methods that prevent the formation of radicals as a result of reaction due to the electrons and holes located on the particle surface. The photocatalytic properties of TiO₂ can be diminished by creating defects in its crystalline lattice to introduce traps for the electrons and holes

generated under the influence of radiation. Hence, the peaks at 431 and 474 nm act as luminescent centers which help to improve the photostability of TiO_2 .

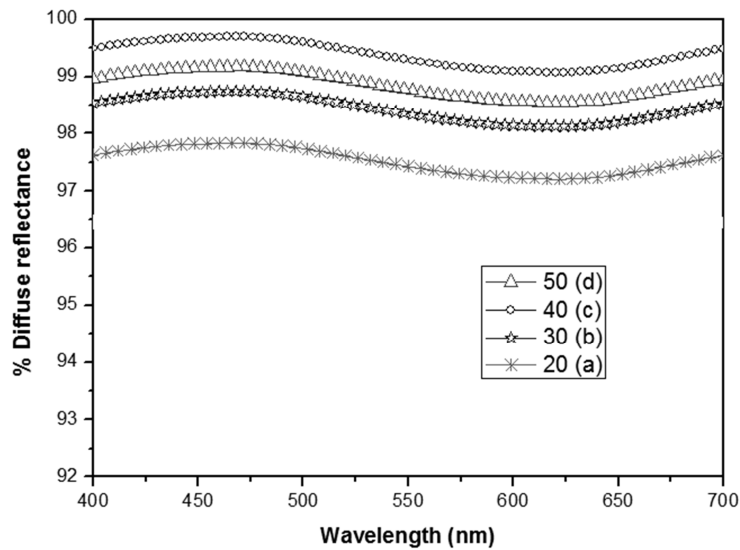


Fig. 8 Diffuse reflectance spectra of TiO_2 nanoparticles calcined at 900°C with different L values (a) 20 (b) 30 (c) 40 (d) 50.

The diffuse reflectance spectra for TiO_2 nanoparticles calcined at 900°C with different L values are shown in Fig. 8. On increasing L from 20 to 40, the diffuse reflectance increases, whereas, it decreases on further increasing L from 40 to 50. These results show attainment of maximum diffuse reflectance (99.50 - 99.60%) with L value of 40 for TiO_2 nanoparticles. As observed from XRD study, with increase in L value (20 - 40), the crystallite size decreases, hence, large is the surface area of particles to scatter light. With further increase in the L value (40 - 50), crystallite size increases which leads to decrease in the surface area and reduces the scattering from the particles. Hence, TiO_2 nanoparticles with L value 40, shows the maximum diffuse reflectance (99.50 - 99.60%). These are potential candidates for the preparation of reflective coatings.

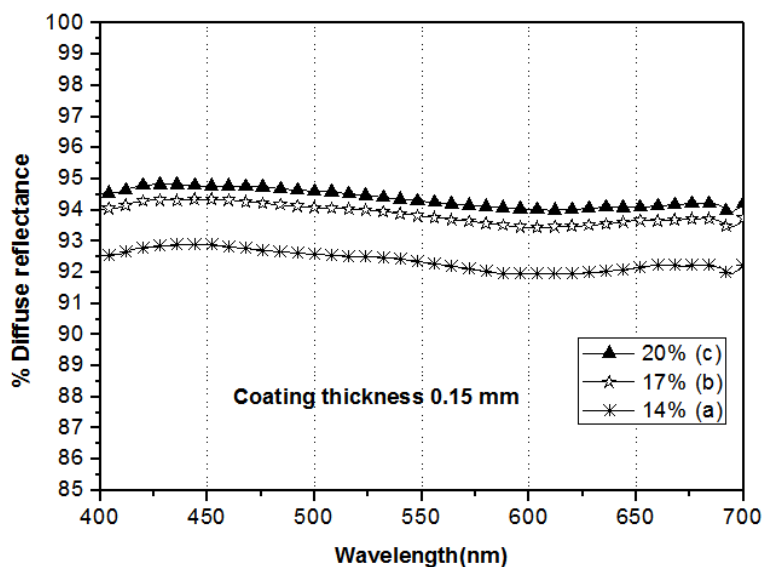


Fig. 9: Diffuse reflectance spectra of the developed reflectors (plastic as substrate) having binder weight ratio.

Fig. 9 shows the diffuse reflectance spectra of the developed reflectors (plastic as substrate) coated with different binder weight ratio. As seen from Fig. 9, with the increase in the binder weight ratio, there is an increase in the diffuse reflectance of the coating. For binder weight ratio from 14 to 17%, the diffuse reflectance increases respectively from 92.56 - 92.40% to 94.05 - 93.88%. With further increase in the binder weight ratio, i.e., from 17 to 20%, there is not much increase in the reflectance. With higher binder weight ratio, there is a strong capillary action between the binder particles, causing them to fuse together and bind TiO₂ nanoparticles into a continuous film.

It has been found that coating material, with less than 14% weight ratio is unable to form stable coating layer and gets easily detached from the plastic sheet. On the other hand, the coating with more than 20% weight ratio, develops cracks; this might be due to the large surface tension of the coating [39].

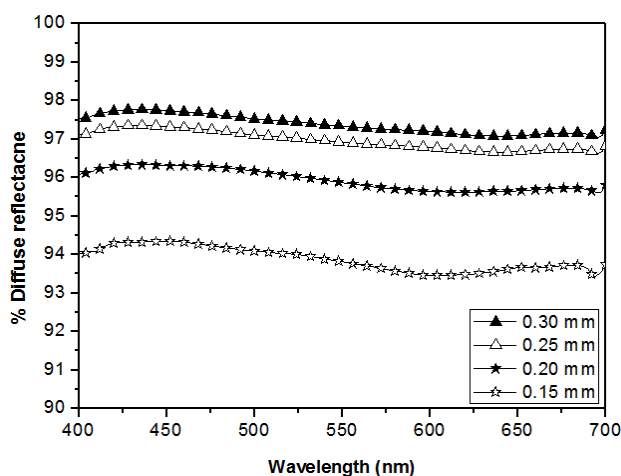


Fig. 10 Diffuse reflectance spectra of the developed reflectors (plastic as substrate) having different coating thicknesses.

Fig. 10 shows the diffuse reflectance of the reflectors (plastic as substrate) with various coating thicknesses. The diffuse reflectance has been found to vary from 94.01 - 93.66%, 96.10 - 95.88%, and 97.12 - 96.91%, respectively, for coating thickness 0.15, 0.20, and 0.25 mm showing that the increase in reflectance is due to high coating thickness; as higher the number of nanoparticles on the substrate more the reflectance. With further increase in thickness, i.e., from 0.25 to 0.30 mm, there is practically no change in the reflectance. Thus, the coating thickness, 0.25 mm, has been found to be the optimum one. At the optimum coating thickness, the critical volume pigment concentration plays an important role in determining reflectance. In general, with increase in the coating thickness, the reflectance increases because greater the film thickness, greater the number of particles on the substrate, which contributes to the higher reflectance. But, there is a particular limit to the concentration of particles in a coating after which there is no increase or little increase in the reflectance (Fig. 10). This limit is determined by critical pigment volume concentration (CPVC) [40, 41].

4. Conclusions

TiO₂ nanoparticles were successfully synthesized and characterized with different characterization techniques. Complete rutile phase formation occurs on calcining the TiO₂ particles at 900°C. On adjusting the ratio of molar concentration of water and alkoxide (L) to 40, the smallest crystallite size of 70.34 nm with particle size 170 nm has been obtained for rutile phase. These particles show the maximum diffuse reflectance, 99.50 - 99.60%. Employing these nanoparticles as reflective pigment and optimizing the pigment to binder ratio and coating thicknesses, the reflectors were successfully developed. These reflectors show the maximum diffuse reflectance, 97.12 - 96.91%, for 0.25-mm thick coating having 17% pigment to binder

weight ratio. The developed reflectors will be of immense use in areas wherever high illumination is required.

Acknowledgements

Sanjeev Kumar is grateful to the Department of Science and Technology, Government of India, for awarding him INSPIRE fellowship to carry out the current research work.

References

- [1] R. H. Fernando, *JCT Coat. Tech.*, **1**(5), 32 (2004).
- [2] S. Kumar, N. K. Verma, M. L. Singla, *J. Coat. Technol. Res.*, **8**(2), 223 (2011).
- [3] D. L. Wang, S. Watson, L. P. Sung, I. H. Tseng, C. J. Bouis, R. Fernando, *J. Coat. Technol. Res.*, **8**(1), 19 (2011).
- [4] K. V. Baiju, S. Shukla, K. S. Sandhya, J. James, K. G. K. Warriar, *J. Phys. Chem. C*, **111**, 7612 (2007).
- [5] N. Eastaugh, V. Walsh, T. Chaplin, R. Siddall, *The Pigment Compendium*, Elsevier Butterworth-Heinemann, Burlington (2004).
- [6] A. K. Ray, S. M. Tracey, B. McQuillin, S. N. B. Hodgson, *IEEE Proc. Sc., Meas. Technol.*, **147**(6), 301 (2000).
- [7] R. J. Tayade, P. K. Surolia, R. G. Kulkarni, R. V. Jasra, *Sci. Technol. Adv. Mater.*, **8**(6), 455 (2007).
- [8] J. A. Pedraza-Avella, R. Lopez, F. Martinez-Ortega, E. A. Paez-Mozo, R. Gomez, *J. Nano. Res.*, **5**(1), 95 (2009).
- [9] W. D. Ross, *Ind. Eng. Chem., Prod. Res. Dev.*, **13**(1): 45 (1974).
- [10] hyperlink:<http://naturalpigments.com/education/article.asp?ArticleID=5>
- [11] hyperlink:<http://naturalpigments.com/education/article.asp?ArticleID=8>
- [12] G. Buxbaum, G. Pfaff, *Industrial Inorganic Pigments*. Wiley-VCH, Strauss GmbH, Morlenbach (2005).
- [13] S. Yin, M. Komatsu, Q. Zhang, F. Saito, T. Sato, *J. Mater. Sci.*, **42**(7), 2399 (2007).
- [14] D. K. Hwang, J. H. Moon, Y. G. Shul, K. T. Jung, D. H. Kim, D. W. Lee, *J. Sol-Gel Sci. Technol.*, **26**(1-3), 783 (2003).
- [15] P. G. Parejo, M. Zayata, D. Levy, *J. Mater. Chem.*, **16**, 2165 (2006).
- [16] Y. Li, P. Leung, L. Yao, Q. W. Song, E. Newton, *J. Hosp. Infect.*, **62**(1), 58 (2006).
- [17] K. Kempa, *Int. J. Nanotechnol.*, **4**(3), 233 (2007).
- [18] B. Finnigan, P. Casey, D. Cookson, P. Halley, K. Jack, R. Truss, D. Martin, *Int. J. Nanotechnol.*, **4**(5), 496 (2007).
- [19] P. Periyat, K. V. Baiju, P. Mukundan, P. K. Pillai, K. G. K. Warriar, *J. Sol-Gel Sci. Technol.*, **43**(3): 299 (2007).
- [20] Y. Zhu, L. Zhang, C. Gao, L. Cao, *J. Mater. Sci.*, **35**(16): 4049 (2000).
- [21] D. P. Macwan, P. N. Dave, S. Chaturvedi, *J. Mater. Sci.*, **46**(11): 3669 (2011).
- [22] A. H. H. Dorian, C. S. Charles, *J. Mater. Sci.*, **46**(4), 855 (2011).
- [23] X. Chen, S. S. Mao, *Chem. Rev.*, **107**(7), 2891 (2007).
- [24] B. Grzmil, M. Rabe, B. Kic, K. Lubkowski, *Ind. Eng. Chem. Res.*, **46**(4): 1018 (2007).
- [25] M. Addamo, V. Augugliaro, A. D. Paola, E. G. Loepez, V. Loddo, G. MarciE, R. Molinari, L. Palmisano, M. Schiavello, *J. Phys. Chem. B*, **108**(10): 3303 (2004).
- [26] M. A. Fox, M. T. Dulay, *Chem. Rev.*, **93**(1), 341 (1993).
- [27] M. Batzill, E. H. Morales, U. Diebold, *Phys. Rev. Lett.*, **96**(2), 26103 (2006).
- [28] R. D. Shannon, J. A. Pask, *J. Am. Cer. Soc.*, **48**(8), 391(1965).
- [29] S. Riyas, G. Krishnan, P. N. Mohandas, *Adv. Appl. Ceram.*, **106**(5), 255 (2007).
- [30] D. G. Syarif, A. Miyashita, T. Yamaki, T. Sumita, Y. Choi, H. Itoh, *App. Surf. Sci.*, **193**(1-4), 287 (2002).
- [31] K. Matsuyama, K. Mishima, K. Hayashi, H. Matsuyama, *J. Nano. Res.*, **5**(1-2), 87 (2003).

- [32] P. I. Gouma, M. J. Mills, *J. Am. Chem. Soc.*, **84**(3), 619 (2001).
- [33] Zachariah, K. V. Baiju, S. Shukla, K. S. Deepa, J. James, K. G. K. Warriar, *J. Phys. Chem. C*, **112**(30), 11345 (2008).
- [34] M. Sharma, S. Kumar, O. P. Pandey, *J. Nano. Res.*, **12**(7), 2655 (2010).
- [35] Y. Cong, J. Zhang, F. Chen, M. Anpo, D. He, *J. Phys. Chem. C*, **111**(28), 10618 (2007).
- [36] M. Yoon, M. Seo, C. Jeong, J. H. Jang, K. S. Jeon, *Chem. Mater.*, **17**(24), 6069 (2005).
- [37] F. Ullmann, *Encyclopedia of Industrial Chemistry*, Wiley-VCH Verlag GmbH, Weinheim (2002).
- [38] A. Zaleska, *Recent Patents on Engineering*, **2**(3): 157 (2008).
- [39] D. Sates, A. A. Tracton, *Coatings Technology Handbook*, 2nd ed., Marcel Dekker, Inc., New York (2001)
- [40] http://goliath.ecnext.com/coms2/gi_0199-3893581/Critical-Pigment-Volume-Concentration-measurements.html
- [41] <http://www.thefreelibrary.com/Critical+Pigment+Volume+Concentration+measurements+...+a+very+fast...-a0130971554>